Two-Photon Interference from a Quantum Emitter in Hexagonal Boron Nitride

Clarisse Fournier, Sébastien Roux, Kenji Watanabe, Takashi Taniguchi, Stéphanie Buil, Julien Barjon, Jean-Pierre Hermier, Aymeric Delteil

Letter

Two-Photon Interference from a Quantum Emitter in Hexagonal Boron Nitride

Clarisse Fournier,[1] Sébastien Roux,[1,2] Kenji Watanabe,[3] Takashi Taniguchi,[4] Stéphanie Buil,[1] Julien Barjon,[1] Jean-Pierre Hermier,[1] and Aymeric Delteil[1,*]

[1] *Université Paris-Saclay, UVSQ, CNRS, GEMaC, 78000 Versailles, France*

[2] *Université Paris-Saclay, ONERA, CNRS, Laboratoire d'étude des microstructures, 92322 Châtillon, France*

[3] *Research Center for Functional Materials, National Institute for Materials Science, 1-1 Namiki, Tsukuba, 305-0044, Japan*

[4] *International Center for Materials Nanoarchitectonics, National Institute for Materials Science, 1-1 Namiki, Tsukuba, 305-0044, Japan*

(Received 11 October 2022; revised 27 March 2023; accepted 31 March 2023; published 27 April 2023)

Recently discovered quantum emitters in 2D materials have opened new prospects for integrated photonic devices for quantum information. Most of these applications require the emitted photons to be indistinguishable, which has remained elusive in 2D materials. Here we investigate two-photon interference of a quantum emitter generated in hexagonal boron nitride with use of an electron beam. We measure the correlations of zero-phonon-line photons in a Hong-Ou-Mandel interferometer under nonresonant excitation. We find that the emitted photons exhibit a partial indistinguishability of 0.44 ± 0.11 in a 3-ns time window, which corresponds to a corrected value of 0.56 ± 0.11 after imperfect emitter purity has been accounting for. The dependence of the Hong-Ou-Mandel visibility on the width of the postselection time window allows us to estimate the dephasing time of the emitter to be approximately 1.5 ns, about half the limit set by spontaneous emission. A visibility greater than 90% is within reach with use of the Purcell effect with current 2D-material photonics.

DOI: 10.1103/PhysRevApplied.19.L041003

Two-photon interference is essential for many photonic implementations of quantum information protocols, from linear optical quantum computing [1] to distant entanglement generation [2–4] and quantum communication [5]. The indistinguishability of two single-photon pulses—which quantifies their ability to interfere—results in the so-called Hong-Ou-Mandel (HOM) effect [6], which refers to the fact that perfectly indistinguishable photons simultaneously reaching the two input ports of a beam splitter always exit the beam splitter from the same output port [7]. Experimental observation of the HOM effect between consecutive photons from a quantum emitter constitutes an important milestone in the use of a physical system for the generation of scalable photonic qubits. Among the physical systems able to generate indistinguishable photons, solid-state single-photon emitters (SPEs) have been widely investigated due to their potential for integration in photonic devices [8]. Thus, photon indistinguishability has been experimentally demonstrated with III-V semiconductor quantum dots [9–12] and color centers in 3D wide-band-gap crystals [13–15].

In turn, recently discovered quantum emitters in 2D materials, comprising trapped excitons in transition-metal dichalcogenides [16–20] and color centers in hexagonal boron nitride (*h*-BN) [21–23], have resulted in growing interest owing to the possibilities of extreme miniaturization and integration into complex heterostructures [24]—yet without demonstration of two-photon interference to date. Among these systems, a recently discovered family of *h*-BN SPEs stands out—a class of blue-emitting color centers (abbreviated as "B centers" in the following) that can be generated at controlled locations with use of an electron beam. Their zero-phonon-line (ZPL) center wavelength is consistently found within 3 meV around 436 nm [25–27]. Several studies have already demonstrated their spectral stability, narrow linewidth, brightness, and single-photon emission up to room temperature [25,26,28].

In this letter, we characterize two-photon interference of light emitted by an individual B center. Our sample consists of a single *h*-BN crystal grown under high-pressure, high-temperature conditions [29] which we exfoliate on a SiO_2(285 nm)/Si substrate. We generate a SPE ensemble in a commercial scanning electron microscope using a slightly defocused electron beam (diameter approximately 300 nm) under 15-kV acceleration voltage and 10-nA current, following Ref. [25] [Fig. 1(a)]. We subsequently

*aymeric.delteil@usvq.fr

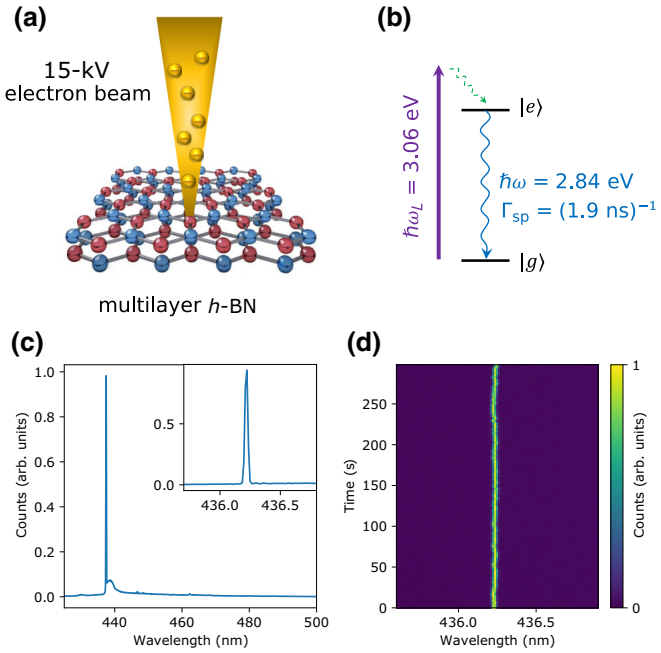

FIG. 1. (a) Irradiation by a 15-kV electron beam generates B centers in a multilayer *h*-BN crystal. (b) Energy levels of the SPE: A 405-nm laser excites the emitter. Nonradiative relaxation occurs, followed by emission of a photon at 436 nm. (c) Low-resolution spectrum of the SPE, where the ZPL and the acoustic phonon sideband can be observed. The inset shows a high-resolution spectrum, limited by the spectrometer resolution of about 100 μeV. The phonon pedestal in the main panel is no longer visible due to the higher resolution. (d) High-resolution spectra as a function of time measured with an integration time of 2 s for 5 min, showing the stability of the SPE.

characterize the sample in a confocal microscope operating in a helium closed-cycle cryostat, keeping the sample at 4 K. The sample is optically excited by a pulsed diode laser of 405-nm wavelength, 850-μW power, and 80-MHz repetition rate [Fig. 1(b)] that is focused on the sample with use of a microscope objective of numerical aperture 0.8. The SPE luminescence is collected through the same objective, and is coupled into a single-mode fiber. In the following, we focus on an individual SPE with a ZPL centered at 436.24 nm. Figure 1(c) shows a low-resolution spectrum of the SPE, exhibiting the usual spectral shape of the B centers, which comprises a narrow ZPL (40% of the emission) and an acoustic phonon sideband (60%). We ensure that spectral diffusion of the ZPL is limited, as shown Fig. 1(d), where the wavelength fluctuations are contained below 20 pm.

Figure 2(a) depicts the experimental setup used for characterization of two-photon interference. The photoluminescence is collected in a single-mode fiber that channels the photons to a delayed Mach-Zehnder interferometer. The ZPL is filtered with use of a transmission grating of 1379 grooves per millimeter. Together with subsequent coupling to single-mode fibers, it implements a narrow-bandpass filter of 100-GHz bandwidth. This spectral width is greater than the time-averaged linewidth but much less than the width of the acoustic phonon sideband of about 7.8 meV (1.9 THz). A polarizer ensures that the input photons have a well-defined linear polarization at the input port of the delayed Mach-Zehnder interferometer. One of the arms is delayed by the same amount as our repetition period (12.5 ns) with use of a 2.6-m fiber, such that two consecutively emitted photons can simultaneously impinge on the beam splitter. A liquid-crystal retarder is inserted in the other arm to rotate the photon polarization by 90° when suited, allowing photon polarization at the two input ports of the second beam splitter to be either identical (parallel) or orthogonal. The total count rate of the ZPL photons at the output ports is about 1200 counts per second. Figure 2(b) shows a histogram of the photon-detection times at the output ports. We first consider photon detections occurring during the $\Delta t =$ 3 ns time window highlighted by the orange shadowing in Fig. 2(b), which is located after the laser pulse of width 550 ps [gray shadowing in Fig. 2(b)]. Figure 2(c) shows the second-order photon correlations measured in a Hanbury Brown–Twiss configuration of the interferometer (i.e., in a single arm). The relative height of the center period allows us to infer a photon purity $g^{(2)}_{\mathrm{HBT}}(0)$ of 0.14 ± 0.03, which is limited by residual background signal and dark counts.

We then measure the photon coincidences in the HOM configuration of the interferometer. Figure 2(d) gives the normalized coincidences measured during 36 h with alternation between parallel and orthogonal polarizations using the liquid-crystal retarder, considering photons detected during the same time window of width Δt. The significant reduction of the center-period value $g^{(2)}_{\mathrm{HOM},\parallel}(0) = 0.32 \pm 0.05$ in the parallel-polarization case as compared with the orthogonal case, $g^{(2)}_{\mathrm{HOM},\perp}(0) = 0.58 \pm 0.07$, is a signature of photon coalescence. The raw (uncorrected) degree of indistinguishability of the emitted photons is then given by the interference visibility defined as $V_{\mathrm{HOM}} = 1 - g^{(2)}_{\mathrm{HOM},\parallel}(0)/g^{(2)}_{\mathrm{HOM},\perp}(0)$. In our case, we find $V_{\mathrm{HOM}} = 0.44 \pm 0.11$. In the case of single photons with ideal purity [i.e., $g^{(2)}_{\mathrm{HBT}}(0) = 0$], V_{HOM} ranges between 0 (perfectly distinguishable photons) and 1 (perfectly indistinguishable photons). When multiple detection events are not negligible, the theoretical bounds of $g^{(2)}_{\mathrm{HOM},\parallel}(0)$ and $g^{(2)}_{\mathrm{HOM},\perp}(0)$ are offset upwards [9], such that the corrected visibility reads $V^{\mathrm{corr}}_{\mathrm{HOM}} = \left(1 + 2g^{(2)}_{\mathrm{HBT}}(0)\right) V_{\mathrm{HOM}}$. In the case of the SPE studied, the theoretical upper (lower) bounds accounting for our finite value of $g^{(2)}_{\mathrm{HBT}}(0)$ are indicated by light (dark) gray bars on the center period of the histogram shown in Fig. 2(d). Accordingly, we find a corrected HOM visibility of $V^{\mathrm{corr}}_{\mathrm{HOM}} = 0.56 \pm 0.11$, which is comparable with the indistinguishability of nonresonantly excited quantum

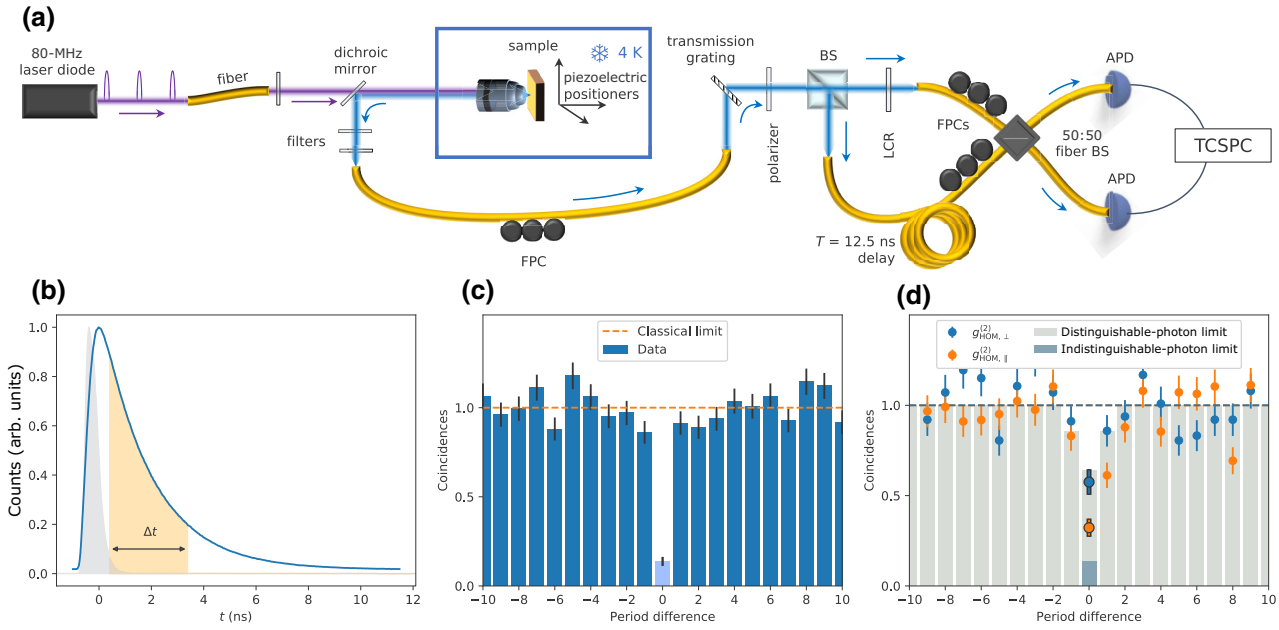

FIG. 2. (a) Experimental setup for the HOM experiment. (b) Histogram of the photon-detection events at the output port. The instrument response function is indicated by the gray shadow. The orange shading of width $\Delta t = 3$ ns indicates the postselection time window. A fit to the data (not shown) provides the spontaneous-emission time $\Gamma_{\rm sp}^{-1} = 1.9$ ns. (c) Second-order correlation function of the photons emitted during Δt, yielding $g^{(2)}(0) = 0.14 \pm 0.03$. The horizontal axis is in the unit of repetition periods. (d) Two-photon coincidences in the Hong-Ou-Mandel configuration. The orange (blue) dots denote the normalized coincidence rate for the parallel-polarization (orthogonal-polarization) configuration of the input ports of the second beam splitter. The center peak provides the values $g^{(2)}_{\rm HOM,\parallel}(0) = 0.32 \pm 0.05$ (parallel case) and $g^{(2)}_{\rm HOM,\perp}(0) = 0.58 \pm 0.07$ (orthogonal case). The light-gray bars mark the theoretical values for distinguishable photons of $g^{(2)}(0) = 0.14$. The dark-gray bar indicates the theoretical value for fully indistinguishable photons of $g^{(2)}(0) = 0.14$. APD, avalanche photodiode; BS, beam splitter; FPC, fiber polarization controller; LCR, liquid-crystal retarder; TCSPC, time-correlated single-photon counter.

dots [9,11] or color centers in wide-gap 3D semiconductors [15]. This observation of HOM interference from single photons emitted by a 2D-material quantum emitter constitutes the main result of our study, and suggests possible practical applications of *h*-BN for optical quantum information, upon further improvement of the visibility.

The limited value of the corrected HOM visibility can be possibly attributed to fast dephasing of the optical dipole. The total dephasing rate of an optical transition can be written as $\gamma = \Gamma_{\rm sp}/2 + \gamma^*$, where $\Gamma_{\rm sp} = 1/T_1$ is the spontaneous emission rate and $\gamma^* = 1/T_2^*$ denotes the rate of dephasing caused by reservoirs other than the vacuum electromagnetic field. In the pulsed regime, only γ^* causes a reduction of the photon indistinguishability [30,31]. An expected consequence of dephasing is that extending the integration window Δt would degrade the HOM visibility by allowing a longer delay time between detected pairs [7,32–35]. It is then in principle possible to estimate γ^* by observing the influence of the postselection time window on the interference visibility. Figure 3(a) (blue dots) plots the measured HOM visibility $V^{\rm corr}_{\rm HOM}$ as a function of the postselection window size Δt. We observe an overall decrease of the HOM visibility as Δt increases, which is consistent with the effect of dephasing. The decay of $V^{\rm corr}_{\rm HOM}(\Delta t)$ can be fitted by an exponential function, of which we fix the intercept to be 1. This result is compatible with the assumption that finite purity and dephasing are the main sources of imperfect HOM visibility. The fit yields the decay time $\tau_V = 2.0$ ns. To relate this timescale to an estimation of γ^*, we simulate the two-photon interference visibility of a two-level atom with dephasing based on numerical integration of a master equation [36–39] accounting for spontaneous emission and dephasing in the Lindblad form. Our simulation accounts for a time postselection of the coincidences in the same way as experimentally realized. The details of the simulation are given in Supplemental Material [40]. We compute the two-photon interference visibility while varying the postselection time window, from which we extract the visibility decay timescale τ_V. By repeating this process for different values of the dephasing rate γ^*, we obtain a one-to-one relation between τ_V and γ^*, which we plot in Fig. 3(b). The dephasing rate associated with our experimental data corresponds to $T_2^* = 2.4 \pm 0.7$ ns, which is in agreement with prior estimations of B-center dephasing time based on the decay of Rabi oscillations in resonant excitation [28], where values of T_2^* between 0.7 and 2 ns were estimated, depending on the emitter and the laser power. In turn, this

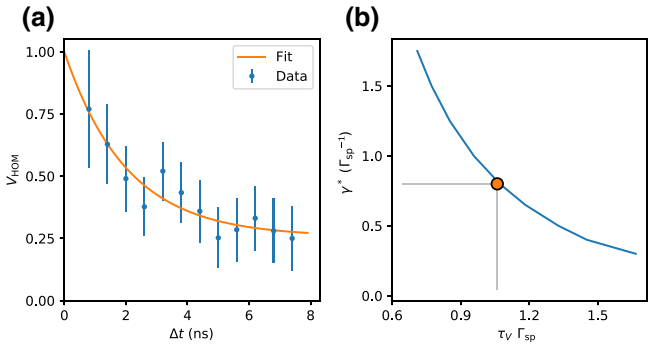

FIG. 3. (a) HOM visibility $V_{\mathrm{HOM}}^{\mathrm{corr}}$ as a function of the postselection time window width Δt shown as blue dots. The orange line is an exponential fit to the data, yielding $\tau_V = 1.7$ ns. (b) Simulated value of τ_V as a function of the dephasing rate γ^* (in the unit of radiative lifetime $\Gamma_{\mathrm{sp}}^{-1}$) shown as the blue line. The orange dot represents the value corresponding to the experimental data in (a).

places the total dephasing time $T_2 = (\Gamma_{\mathrm{sp}}/2 + \gamma^*)^{-1} = 1.5$ ns about halfway from the perfect indistinguishability limit, $T_2 = 2T_1 = 3.8$ ns.

The value of indistinguishability we measure could be further increased by use of resonant excitation, which selectively addresses the transition of interest. This leads to a decrease of the saturation power by several orders of magnitude and therefore of the environment noise, yielding up to Fourier-limited linewidths [41]. Additionally, embedding the emitter in a cavity would increase the ratio between the rates of spontaneous emission and dephasing. We calculate that a Purcell factor of 7 (15) would increase the indistinguishability to 80% (90%), while increasing at the same time the collection efficiency. Similar or greater spontaneous-emission enhancements have been achieved in 2D materials [42,43]. Integrating B centers into electrical gates for fine-tuning of the optical resonance would then allow interference between distinct emitters [44]. The indistinguishability of photons emitted by *h*-BN B centers, together with their already-established advantageous photophysical properties and the possibility to locate them at a prechosen position, opens the way to a broad range of applications in integrated quantum photonics and optical quantum information based on 2D materials.

ACKNOWLEDGMENTS

The authors acknowledge Aurélie Pierret and Michael Rosticher for the flake exfoliation. This work was supported by the French Agence Nationale de la Recherche under reference ANR-21-CE47-0004-01 (E−SCAPE project). This work also received funding from the European Union's Horizon 2020 research and innovation program under Grant No. 881603 (Graphene Flagship Core 3). K.W. and T.T. acknowledge support from Japan Society for the Promotion of Science Grants-in-Aid for Scientific Research (KAKENHI) (Grants No. 19H05790, No. 20H00354, and No. 21H05233).

[1] E. Knill, R. Laflamme, and G. J. Milburn, A scheme for efficient quantum computation with linear optics, Nature **409**, 46 (2001).
[2] C. Cabrillo, J. I. Cirac, P. García-Fernández, and P. Zoller, Creation of entangled states of distant atoms by interference, Phys. Rev. A **59**, 1025 (1999).
[3] H. Bernien, B. Hensen, W. Pfaff, G. Koolstra, M. S. Blok, L. Robledo, T. H. Taminiau, M. Markham, D. J. Twitchen, L. Childress, and R. Hanson, Heralded entanglement between solid-state qubits separated by three metres, Nature **497**, 86 (2013).
[4] A. Delteil, Z. Sun, W.-B. Gao, E. Togan, S. Fält, and A. Imamoğlu, Generation of heralded entanglement between distant hole spins, Nat. Phys. **12**, 218 (2016).
[5] N. Gisin and R. Thew, Quantum communication, Nat. Photon. **1**, 165 (2007).
[6] C. K. Hong, Z. Y. Ou, and L. Mandel, Measurement of Subpicosecond Time Intervals between Two Photons by Interference, Phys. Rev. Lett. **59**, 2044 (1987).
[7] F. Bouchard, A. Sit, Y. Zhang, R. Fickler, F. M. Miatto, Y. Yao, F. Sciarrino, and E. Karimi, Two-photon interference: The Hong–Ou–Mandel effect, Rep. Prog. Phys. **84**, 012402 (2021).
[8] I. Aharonovich, D. Englund, and M. Toth, Solid-state single-photon emitters, Nat. Photon. **10**, 631 (2016).
[9] C. Santori, D. Fattal, J. Vučković, G. S. Solomon, and Y. Yamamoto, Indistinguishable photons from a single-photon device, Nature **419**, 594 (2002).
[10] N. Somaschi, V. Giesz, L. De Santis, J. C. Loredo, M. P. Almeida, G. Hornecker, S. L. Portalupi, T. Grange, C. Antón, J. Demory, C. Gómez, I. Sagnes, N. D. Lanzillotti-Kimura, A. Lemaítre, A. Auffeves, A. G. White, L. Lanco, and P. Senellart, Near-optimal single-photon sources in the solid state, Nat. Photonics **10**, 340 (2016).
[11] A. Thoma, P. Schnauber, J. Böhm, M. Gschrey, J.-H. Schulze, A. Strittmatter, S. Rodt, T. Heindel, and S. Reitzenstein, Two-photon interference from remote deterministic quantum dot microlenses, Appl. Phys. Lett. **110**, 011104 (2017).
[12] W.-B. Gao, P. Fallahi, E. Togan, A. Delteil, Y. S. Chin, J. Miguel-Sanchez, and A. Imamoğlu, Quantum teleportation from a propagating photon to a solid-state spin qubit, Nat. Commun. **4**, 2744 (2013).
[13] A. Sipahigil, M. L. Goldman, E. Togan, Y. Chu, M. Markham, D. J. Twitchen, A. S. Zibrov, A. Kubanek, and M. D. Lukin, Quantum Interference of Single Photons from Remote Nitrogen-Vacancy Centers in Diamond, Phys. Rev. Lett. **108**, 143601 (2012).
[14] A. Sipahigil, K. D. Jahnke, L. J. Rogers, T. Teraji, J. Isoya, A. S. Zibrov, F. Jelezko, and M. D. Lukin, Indistinguishable Photons from Separated Silicon-Vacancy Centers in Diamond, Phys. Rev. Lett. **113**, 113602 (2014).
[15] N. Morioka, N. Morioka, C. Babin, R. Nagy, I. Gediz, E. Hesselmeier, D. Liu, M. Joliffe, M. Niethammer, D. Dasari,

V. Vorobyov, R. Kolesov, R. Stöhr, J. Ul-Hassan, N. T. Son, T. Ohshima, P. Udvarhelyi, G. Thiering, A. Gali, J. Wrachtrup, and F. Kaiser, Spin-controlled generation of indistinguishable and distinguishable photons from silicon vacancy centres in silicon carbide, Nat. Commun. **11**, 2516 (2020).

[16] C. Chakraborty, L. Kinnischtzke, K. M. Goodfellow, R. Beams, and A. N. Vamivakas, Voltage-controlled quantum light from an atomically thin semiconductor, Nat. Nanotechnol. **10**, 507 (2015).

[17] Y.-M. He, G. Clark, J. R. Schaibley, Y. He, M.-C. Chen, Y.-J. Wei, X. Ding, Q. Zhang, W. Yao, X. Xu, Chao-Yang Lu, and Jian-Wei Pan, Single quantum emitters in monolayer semiconductors, Nat. Nanotechnol. **10**, 497 (2015).

[18] M. Koperski, K. Nogajewski, A. Arora, V. Cherkez, P. Mallet, J.-Y. Veuillen, J. Marcus, P. Kossacki, and M. Potemski, Single photon emitters in exfoliated WSe_2 structures, Nat. Nanotechnol. **10**, 503 (2015).

[19] A. Srivastava, M. Sidler, A. V. Allain, D. S. Lembke, A. Kis, and A. Imamoğlu, Optically active quantum dots in monolayer WSe_2, Nat. Nanotechnol. **10**, 491 (2015).

[20] P. Tonndorf, R. Schmidt, R. Schneider, J. Kern, M. Buscema, G. A. Steele, A. Castellanos-Gomez, H. S. J. van der Zant, S. Michaelis de Vasconcellos, and R. Bratschitsch, Single-photon emission from localized excitons in an atomically thin semiconductor, Optica **2**, 347 (2015).

[21] T. T. Tran, K. Bray, M. J. Ford, M. Toth, and I. Aharonovich, Quantum emission from hexagonal boron nitride monolayers, Nat. Nanotechnol. **11**, 37 (2016).

[22] R. Bourrelier, S. Meuret, A. Tararan, O. Stéphan, M. Kociak, L. H. G. Tizei, and A. Zobelli, Bright UV single photon emission at point defects in h-BN, Nano Lett. **16**, 4317 (2016).

[23] L. J. Martínez, T. Pelini, V. Waselowski, J. R. Maze, B. Gil, G. Cassabois, and V. Jacques, Efficient single photon emission from a high-purity hexagonal boron nitride crystal, Phys. Rev. B **94**, 121405 (2016).

[24] A. K. Geim and I. V. Grigorieva, Van der Waals heterostructures, Nature **499**, 419 (2013).

[25] C. Fournier, A. Plaud, S. Roux, A. Pierret, M. Rosticher, K. Watanabe, T. Taniguchi, S. Buil, X. Quélin, J. Barjon, J.-P. Hermier, and A. Delteil, Position-controlled quantum emitters with reproducible emission wavelength in hexagonal boron nitride, Nat. Commun. **12**, 3779 (2021).

[26] A. Gale, C. Li, Y. Chen, K. Watanabe, T. Taniguchi, I. Aharonovich, and M. Toth, Site-specific fabrication of blue quantum emitters in hexagonal boron nitride, ACS Photonics **9**, 2170 (2022).

[27] B. Shevitski, M. Gilbert, C. T. Chen, C. Kastl, E. S. Barnard, E. Wong, D. F. Ogletree, K. Watanabe, T. Taniguchi, A. Zettl, and S. Aloni, Blue-light-emitting color centers in high-quality hexagonal boron nitride, Phys. Rev. B **100**, 155419 (2019).

[28] J. Horder, S. White, A. Gale, C. Li, K. Watanabe, T. Taniguchi, M. Kianinia, I. Aharonovich, and M. Toth, Coherence Properties of Electron-Beam-Activated Emitters in Hexagonal Boron Nitride under Resonant Excitation, Phys. Rev. Appl. **18**, 064021 (2022).

[29] T. Taniguchi and K. Watanabe, Synthesis of high-purity boron nitride single crystals under high pressure by using Ba–BN solvent, J. Cryst. Growth **303**, 525 (2007).

[30] J. Bylander, I. Robert-Philip, and I. Abram, Interference and correlation of two independent photons, Eur. Phys. J. D **22**, 295 (2003).

[31] A. Kiraz, M. Atatüre, and A. Imamoğlu, Quantum-dot single-photon sources: Prospects for applications in linear optics quantum-information processing, Phys. Rev. A **69**, 032305 (2004).

[32] J. A. Martínez, R. A. Parker, K. C. Chen, M. Purser, L. Li, C. P. Michaels, A. M. Stramma, R. Debroux, I. B. Harris, M. H. Appel, *et al.*, Photonic Indistinguishability of the Tin-Vacancy Center in Nanostructured Diamond, Phys. Rev. Lett. **129**, 173603 (2022).

[33] R. Proux, M. Maragkou, E. Baudin, C. Voisin, P. Roussignol, and C. Diederichs, Measuring the Photon Coalescence Time Window in the Continuous-Wave Regime for Resonantly Driven Semiconductor Quantum Dots, Phys. Rev. Lett. **114**, 067401 (2015).

[34] J.-H. Kim, T. Cai, C. J. K. Richardson, R. P. Leavitt, and E. Waks, Two-photon interference from a bright single-photon source at telecom wavelengths, Optica **3**, 577 (2016).

[35] C. Nawrath, F. Olbrich, M. Paul, S. L. Portalupi, M. Jetter, and P. Michler, Coherence and indistinguishability of highly pure single photons from non-resonantly and resonantly excited telecom C-band quantum dots, Appl. Phys. Lett. **115**, 023103 (2019).

[36] R. Loudon, *The Quantum Theory of Light* (Oxford University Press, New York, 1983), 2nd ed.

[37] K. A. Fischer, K. Müller, K. G. Lagoudakis, and J. Vučković, Dynamical modeling of pulsed two-photon interference, New J. Phys. **18**, 113053 (2016).

[38] J. R. Johansson, P. D. Nation, and F. Nori, QuTiP: An open-source Python framework for the dynamics of open quantum systems, Comput. Phys. Commun. **183**, 1760 (2012).

[39] J. R. Johansson, P. D. Nation, and F. Nori, QuTiP 2: A Python framework for the dynamics of open quantum systems, Comput. Phys. Commun. **184**, 1234 (2013).

[40] See Supplemental Material at http://link.aps.org/supplemental/10.1103/PhysRevApplied.19.L041003 for the details of the simulations of time-gated two-photon interference.

[41] C. Fournier, K. Watanabe, T. Taniguchi, S. Buil, J. Barjon, J.-P. Hermier, and A. Delteil, Investigating the fast spectral diffusion of a quantum emitter in hBN using resonant excitation and photon correlations, arXiv:2303.05315 (2023).

[42] J. E. Fröch, C. Li, Y. Chen, M. Toth, M. Kianinia, S. Kim, and I. Aharonovich, Purcell enhancement of a cavity-coupled emitter in hexagonal boron nitride, Small **18**, 2104805 (2021).

[43] O. Iff, Q. Buchinger, M. Moczała-Dusanowska, M. Kamp, S. Betzold, M. Davanco, K. Srinivasan, S. Tongay, C. Antń-Solanas, S. Höfling, and C. Schneider, Purcell-enhanced single photon source based on a deterministically placed WSe_2 monolayer quantum dot in a circular Bragg grating cavity, Nano Lett. **21**, 4715 (2021).

[44] I. Zhigulin, J. Horder, V. Ivady, S. J. U. White, A. Gale, C. Li, C. J. Lobo, M. Toth, I. Aharonovich, and M. Kianinia, Stark Effect of Blue Quantum Emitters in Hexagonal Boron Nitride, Phys. Rev. Appl. **19**, 044011 (2023).